Halogen bonding: an underestimated player in membrane–ligand interactions

Rafael Santana Nunes,[†,‡] Diogo Vila-Viçosa,[†,¶] and Paulo J. Costa[*,†]

†University of Lisboa, Faculty of Sciences, BioISI - Biosystems & Integrative Sciences Institute, Campo Grande, C8 bdg, 1749-016 Lisboa, Portugal

‡Centro de Química Estrutural, Faculdade de Ciências, Universidade de Lisboa, Campo Grande, 1749-016 Lisboa, Portugal

¶Current address: Kinetikos, Coimbra, Portugal

E-mail: pjcosta@ciencias.ulisboa.pt,pjcosta@fc.ul.pt

Phone: +351-21-7500845

Abstract

Halogen bonds (XBs) are noncovalent interactions where halogen atoms act as electrophilic species interacting with Lewis bases. These interactions are relevant in biochemical systems being increasingly explored in drug discovery, mainly to modulate protein–ligand interactions, but are also found in engineered protein or nucleic acid systems. In this work, we report direct evidence for the existence of XBs in the context of biological membrane systems thus expanding the scope of application of these interactions. Indeed, our molecular dynamics simulations show the presence of favorable interactions between halobenzene derivatives and both phosphate or ester oxygen acceptors from model phospholipid bilayers, thus supporting the existence of XB-mediated phospholipid–halogen recognition phenomena influencing the membrane insertion profile of the ligands and their orientational preferences. This represents a relevant interaction, previously overlooked, eventually determining the pharmacological

or toxicological activity of halogenated compounds and hence with potential implications in drug discovery and development, a place where such species account for a significant part of the chemical space. We also provide insights into a potential role for XBs in water-to-membrane insertion of halogenated ligands as XBs are systematically observed during this process. Therefore, our data strongly suggests that, as the ubiquitous hydrogen bond, XBs should be accounted for in the development of membrane partition models.

keywords: halogen bonding, phospholipid–ligand interactions, biomolecular recognition, membrane permeation, molecular dynamics simulations

Introduction

Proteins and nucleic acids are the most common targets of bioactive molecules or drugs towards therapeutic applications.[1] Despite the development of strategies aiming at membrane receptors,[2] specific targeting of the membrane phospholipids is much less common. However, in the last few years, new therapeutic approaches have been developed in which lipids are specifically addressed, i.e. membrane-lipid therapy.[3] Indeed, many bioactive compounds and drug(-like) molecules are membrane-active, interacting directly with membrane lipids, modulating its biophysical properties, and eventually triggering subsequent downstream events that lead to promiscuous cellular alterations.[4–7] This interaction is often concomitant with specific therapeutical effects[3] such as in the case of antimicrobial peptides,[8–10] sugar-based bactericides[11] and other small molecule antibiotics,[12] or modulators of multidrug resistance of tumoral cells.[13] Besides therapeutical effects, the interaction of small molecules with membranes might also be responsible for their nonspecific toxicity. For instance, the toxic effects of poly-halogenated biphenyls[14] or brominated flame retardants[15] were ascribed in part to their membrane-binding and perturbing effects.[15,16] Therefore, understanding lipid–ligand interactions is paramount not only for designing the above-mentioned lipid therapies[3] or

<div align="center">2</div>

to assess the toxicity of compounds, but also to describe phenomena such as membrane permeability, which plays a key role in drug design and development.[17–21]

The interaction and/or diffusion of a drug through a membrane is dependent on a variety of factors, among them, its ability to establish noncovalent interactions. In this scope, the formation of intra- or intermolecular hydrogen bonds (HBs) is a well known crucial factor affecting membrane–ligand interactions and permeability, hence determining pharmacological activity.[22–26] In contrast, the role of other noncovalent interactions, in particular, halogen bonds (XBs),[27] remains unaddressed in the field of membrane–ligand recognition.

XBs consist of R–X$\cdots$B (X = Cl, Br, or I; B = Lewis base; R = substituent) noncovalent interactions that are predominantly explained by the existence of a localized region of depleted electron density at the tip of the covalently-bound halogen atom named σ–hole.[28] XBs have found application in many fields across the chemical and material sciences,[29,30] and also in biology. Indeed, since the seminal work of P. Shing Ho and co-workers,[31] they have been recognized as important players in biomolecular recognition phenomena in protein[32,33] or nucleic acid[34–40] systems, and, consequently, have been successfully employed as tools in medicinal chemistry.[41–43] However, to the best of our knowledge, no reports exist on specific XB-mediated membrane–ligand recognition phenomena. This is surprising since halogen atoms, present in c.a. 25% of marketed drugs and being even more prevalent in earlier stages of drug discovery and development processes,[44] have traditionally been employed in rational drug design to improve the pharmacokinetic profile of lead molecules, namely to enhance passive diffusion across membranes[45] or, as recently shown, to increase the receptor-mediated uptake of small fluorescent molecules[46,47] or proteins[48] by mammalian cells.[49] Also, iodination of polymers increases their cellular uptake by plant cells, an effect attributed to XBs.[50] None of the above reports, however, specifically addressed XB-mediated passive diffusion. On the other hand, recent experimental work addressing the substituent effects on the membrane penetration properties of substituted biphenyls showed that the substituted ring is preferably located at the apolar/polar interface, an effect attributed to

the stabilization effect of XBs between chloride and a lipid phosphate oxygen.[51] Although a direct experimental observation could not be obtained, this hypothesis was supported by QM calculations on a model p-chlorobiphenyl$\cdots$PO$_2$(OMe)$_2$ dimer.

Indeed, several indirect pieces of evidence such as the above point out to the potential existence of XB-mediated lipid–ligand interactions. XBs are observed in solution,[52] including in aqueous media,[53,54] and can be exploited in the design of synthetic transmembrane anion transporters with potential therapeutic applications. This concept, initially reported by Matile and co-workers[55] was further developed[56–58] exploring also other noncovalent interactions.[59,60] As for anion transporters that are known to interact directly with lipid membranes by establishing HBs with several nucleophilic sites from the phospholipid headgroups, i.e. oxygen atoms,[61–63] halogen-bonding anion transporters, or any other XB-donor molecule, may eventually engage in an interaction with those sites as well (Figure 1a). Those sites, divided into two dynamic outer membrane regions with the phosphate oxygen (PO) acceptors more exposed to water and the ester oxygen (CO) acceptors located closer to the membrane core (Figure 1b, green and blue, respectively), bear resemblances with previously reported XB acceptors. Indeed, concerning CO-type acceptors, carbonyl oxygens from the protein backbone are frequent and easily targeted XB acceptors,[31,64,65] while in the case of PO interaction sites, the oxygen atoms of phosphines and phosphates are known XB acceptors,[66–71] the most remarkable case being the phosphate oxygens from nucleic acids.[31,34,38] In addition, it was recently shown that both HB and XB interactions participate in the stabilization of complexes between halothane, a well known volatile anesthetic agent, and a lipid phosphate acceptor model (hexamethylphosphortriamide), both in the solid-state and in solution.[70] This study supported the concept that XBs might play a role, similarly to HBs, in the molecular recognition of drugs and other small molecules by phospholipids from cell membranes. Finally, preliminary QM calculations using halobenzenes with dimethyl phosphate and methyl acetate as models for PO- and CO-type biomolecular acceptors, respectively, indicate the formation of stable complexes (Table S1).
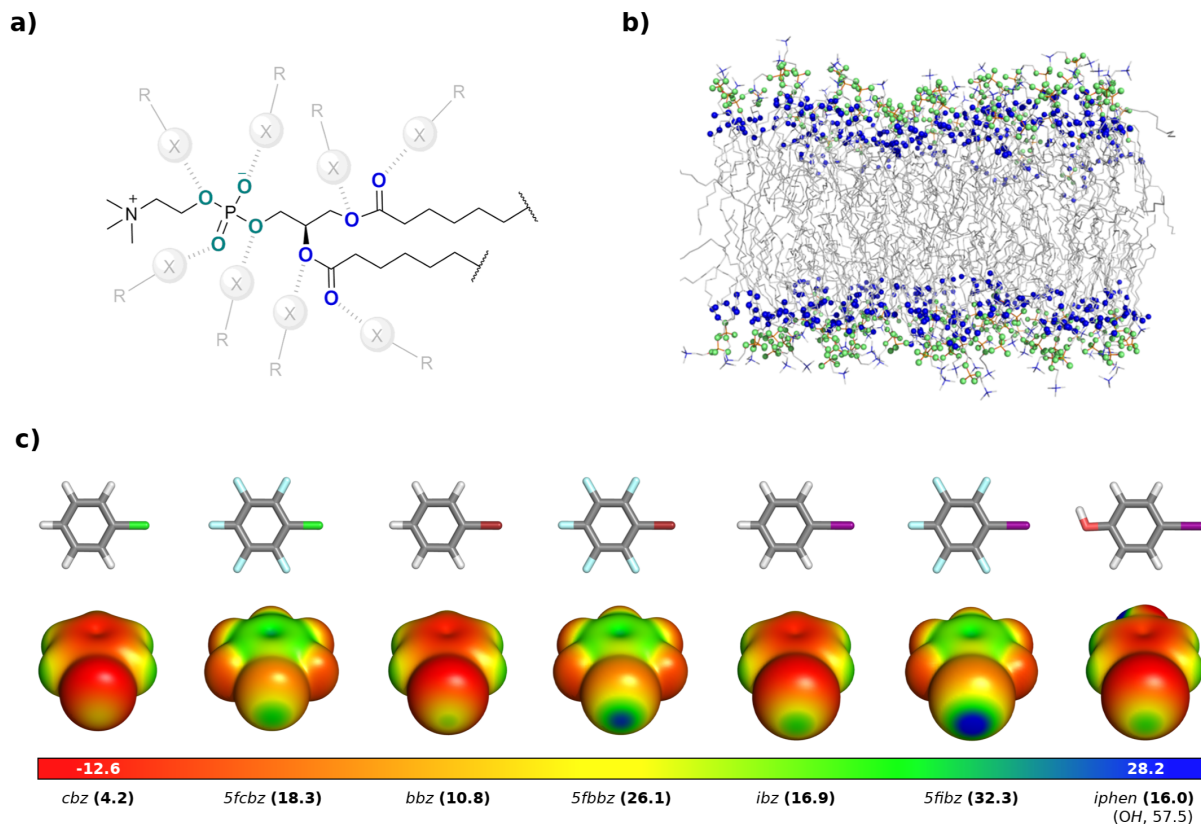
Figure 1: (a) Representation of a phosphatidylcholine (PC) molecule highlighting the different lipid XB- (or HB-) acceptor sites (X = Cl, Br, I or OH; R = substituent); (b) PO-(green) and CO-type (blue) acceptor layers in a representative POPC bilayer; (c) Halobenzene derivatives studied in this work, namely, chlorobenzene (*cbz*), chloropentafluorobenzene (*5fcbz*), bromobenzene (*bbz*), bromopentafluorobenzene (*5fbbz*), iodobenzene (*ibz*), iodopentafluorobenzene (*5fibz*), and 4-iodophenol (*iphen*), their molecular electrostatic potentials (ESPs) mapped on the 0.001 au contour of the electron density (values in kcal mol^{-1}), and $V_{\max}$ (in parentheses) at the halogen (and OH for *iphen*) computed at the B3LYP/6-311G(d,p) level.

Despite all the above-mentioned data suggesting the occurrence of membrane–small molecule XB interactions, no direct evidence, similar to that gathered for proteins and nucleic acids[31–33,38,72] has been reported yet. The identification of the targets of small molecules by experimental techniques, although crucial, is not an easy task[73] and, in this particular case, identifying an XB in a fluid membrane environment might be challenging to achieve experimentally by standard techniques. The existence of such interaction might open an avenue for future drug design or developments in toxicology, specifically when lipids are di-

rectly targeted.[3] In this context, *in silico* methods may provide useful insights into the study of these events at the molecular level.

Herein, we present the first account addressing halogen bonding in membrane–ligand interactions, highlighting their role in mediating the recognition phenomena and on the distribution of halogenated compounds along phospholipid membranes. A possible role for XBs in the water-to-membrane insertion mechanism is also discussed. This was accomplished using molecular mechanics / molecular dynamics (MM/MD) simulations, explicitly accounting for the σ–hole in halogenated species (see Methods), using a model POPC bilayer, together with a series of halobenzene derivatives (Figure 1c) that are commonly used as probes to evaluate the XB-capability of small molecules in MD simulations of protein–ligand systems.[74–76]

Given the significant part of the chemical space occupied by halogenated molecules in the framework of drug discovery and development, we hope to provide new tools for rational drug design and/or *in silico* toxicology, also contributing to improve the commonly used molecular descriptors for membrane partition models.

Methods

Model Systems

To study the potential role of XBs in membrane–ligand recognition phenomena, the cell membrane was modeled as a 1-palmitoyl-2-oleoyl-*sn*-glycero-3-phosphocholine (POPC) bilayer.[61–63] A series of halobenzene derivatives (Figure 1c), capable of establishing XBs and with different partition coefficients (log K_{OW}), were chosen as probes, in the attempt to cover the wide range of halogenated species present in drug-like molecules (iodinated, brominated, and, most frequently, chlorinated compounds[44]). Concerning iodinated probes, iodopentafluorobenzene ($5fibz$, log $K_{OW} = 3.54$[77,78]), exhibiting a considerable σ–hole corresponding to a local maximum on the electrostatic potential ($V_{\max}$) of 32.3 kcal mol^{-1} (B3LYP/6-311G(d,p)) and a XB-mediated transmembrane anion transport activity (EC$_{50}$)

of 260 μM[55] was selected as a strong XB donor probe together with iodobenzene (ibz) which is a considerably weaker XB donor ($V_{\max} = 16.9$ kcal mol^{-1}), exhibits much negligible transmembrane anion transport activity (EC$_{50} > 2$ mM),[55] and a lower log K_{OW} value (3.25)[79] In addition, 4-iodophenol ($iphen$), which is also a weak XB donor ($V_{\max} = 16.0$ kcal mol^{-1}) and with the lowest hydrophobicity amongst the studied iodinated molecules (log $K_{OW} = 2.91$),[78] was selected as a model halogen- and hydrogen-bonding probe to inspect the competing effect of the two intermolecular interactions. Notice that XBs and HBs have a complex relationship, either competing, replacing, or behaving independently from each other.[30,80] A similar rational was followed for the remainder molecules. Bromobenzene (bbz, $V_{\max} = 10.8$ kcal mol^{-1}, log $K_{OW} = 2.99$[79]) and bromopentafluorobenzene ($5fbbz$, $V_{\max} = 26.1$ kcal mol^{-1}, log $K_{OW} = 3.33$[77,78]) were used as brominated probes, the latter molecule presenting a transmembrane anion transport activity (EC$_{50}$) of 1.9 mM,[55] whereas in the case of chlorinated probes, chlorobenzene (cbz, $V_{\max} = 4.2$ kcal mol^{-1}, log $K_{OW} = 2.77$[79]) and chloropentafluorobenzene ($5fcbz$, $V_{\max} = 18.3$ kcal mol^{-1}, log $K_{OW} = 3.18$[77,78]) were used.

Probe Parametrization

To account for XBs in MM/MD simulations, the halobenzene derivatives were parameterized employing an extra-point (EP) model[81–84] implemented in the context of the general AMBER force field (GAFF).[85] In this approach, the halogen atom is modeled by introducing a positively charged particle (EP) mimicking the σ–hole, thus emulating the charge anisotropy. This strategy was successfully applied in a variety of computational studies of XB-mediated biomolecular recognition using MD simulations,[86–89] including variants of the original parametrization.[74,75,90,91] The EP is commonly located at a distance from the halogen (X) corresponding to its Lennard-Jones (LJ) parameter $R_{\min}$ (i.e. $d_{\mathrm{X-EP}} = R_{\min}$) and atomic partial charges are subsequently derived for all atoms by a restrained electrostatic potential (RESP)[92] fitting procedure, although other authors have proposed alternative EP parametrization schemes in the same context.[93–97] The EP approach is easily ported to

other force fields,[43] namely OPLS,[98–100] CHARMM[101] or GROMOS,[76] and is compatible with Poisson–Boltzmann and surface area (PBSA)[102,103] or generalized Born (GBSA)[104,105] calculations for estimating protein–ligand binding free energy or hydration free energies. Notice that, despite other less standard approaches being available,[43,106] including force fields specifically designed for biological applications,[107,108] based on QM data,[109] or featuring explicit terms to account for polarization effects,[110–112] these however are not easily generalized for standard force fields.

Accordingly, the molecular electrostatic potential (ESP) at the HF/6-31G(d)[113–115] level of theory (6-311G(d)[116] basis set in the case of iodine) was generated for the halobenzene molecules, previously optimized at the B3LYP/6-311G(d,p) level of theory, using Gaussian 09.[117] The atomic radius of iodine was set to 2.3 Å,[118] similarly to previous work,[76,103] while default Merz-Singh-Kollman (MK) radii were employed for the remaining elements. The calculations were performed using four concentric layers of points per atom and six points per unit area with the input options `IOp(6/33 = 2, 6/41 = 4, 6/42 = 6)`. An EP was then introduced along the C–X covalent bond axis, with the C–X–EP angle fixed at 180.0° and a X–EP distance of 1.948, 2.020, or 2.150 Å for chloride, bromide, or iodine, respectively, which corresponds to the R_{min} value for these atoms in current versions of GAFF, as previously noted.[43,103] Atomic partial charges were subsequently derived by RESP, which was carried out using the `antechamber`[119] module as implemented in AmberTools 15,[120] thus generating models cbz^{EP}, $5fcbz^{\mathrm{EP}}$, bbz^{EP}, $5fbbz^{\mathrm{EP}}$, ibz^{EP}, $5fibz^{\mathrm{EP}}$, and $iphen^{\mathrm{EP}}$. Probe topologies were generated by assigning GAFF atom types with the `leap` tool (AmberTools 15), and converted into GROMACS-compatible format using the `acpype`[121] tool. The EPs were modeled as GROMACS type 2 virtual sites defined by the respective C–X bond, and without additional parameters, similar to previous work.[76] The full sets of charges (Figure S1a) and final topology files (`.itp` format) are provided as Supporting Information. Note that the parameters used herein are able to satisfactorily reproduce at the MM level the geometries of XB interactions between halobenzenes and dimethyl phosphate or methyl acetate

(as a model for PO- and CO-type acceptors, respectively) calculated at the M062X/def2-TZVP level of theory (Table S1), especially when considering the zwitterionic nature of the phosphatidylcholine moiety, reflected in the high charges of the phosphate oxygen atoms in the Lipid14 parameter set (Figure S1b) when compared with the neutral model acceptors.

System Setup

The systems were built from a pre-equilibrated POPC bilayer containing 128 lipids solvated with 5652 water molecules. As mentioned above, halobenzene molecules were selected as probes to assess different phospholipid–halogen interactions and their relative preferences. Individual simulations of each system were performed by adding two probe molecules either into the interior of the lipid bilayer or in the water phase (Figure S2). Several simulation replicates were run for each setup. For all systems and replicates, we observed that, in the first scenario, the halobenzenes remained inserted in the lipid phase throughout all the simulation time while in the second case, the molecules inserted into the bilayer at different time scales, remaining inserted during the remainder simulation time (Figures S3-S9). After insertion, the simulations are in equilibrium and both scenarios are indistinguishable. The first 45 ns of the simulation (when starting from the membrane core) or the time prior to insertion (starting from the water phase) were discarded as equilibration time. Since the two probe molecules do not aggregate and typically do not interact with each other, each corresponding trajectory was also treated separately as individual replicates for analysis purposes. Overall, statistics was performed over 10 individual replicates of 160 ns each, yielding a total of 1.6 μs of sampling time for each system. The time evolution of all replicates and the 160 ns segments used for analysis are highlighted in Figures S3-S9. Since we were also interested in the potential XB-mediated insertion process, the non-equilibrium segments of the previously mentioned simulations (with the probes starting in the water phase and subsequently inserting into the membrane) were also analyzed. For this purpose, additional simulations starting from the water phase were performed until 10 replicates of individual

insertion events were sampled for each halobenzene–POPC system.

MM/MD Settings

Molecular mechanics/molecular dynamics (MM/MD) simulations were performed using the GROMACS software package, versions 5.1.2 and 5.1.5.[122–124] The AMBER lipid FF (Lipid14 release)[125] was used for POPC together with TIP3P[126] for water, as described in ref. 125. The halobenzene molecules were modeled in the framework of GAFF[85] (with or without an EP), as described above. A tetragonal simulation box was employed, using three-dimensional periodic boundary conditions with the minimum image convention. The simulations were performed in an isothermal-isobaric (NPT) ensemble, with the temperature maintained at 303 K using the velocity-rescale algorithm[127] and a coupling constant of 0.1 ps, while pressure was kept constant at 1 bar using a semi-isotropic Berendsen barostat,[128] in which the x and y directions are coupled together whereas the z direction is treated separately, as in the original Lipid14 parametrization,[125] with a coupling constant of 1.0 ps and an isothermal compressibility of 4.5×10^{-5} bar^{-1}. Electrostatic interactions were treated using the smooth particle mesh Ewald (PME) method[129,130] with a Fourier grid spacing of 0.16 nm and a real-space cutoff of 1.0 nm. Lennard-Jones interactions were truncated at 1.0 nm. The buffered Verlet list scheme[131] was used for neighbor searching.

The parallel version of the linear constraint solver (P-LINCS)[132,133] algorithm was used to constrain all lipid and probe bonds, while the SETTLE[134] algorithm was used for water. Energy minimization was performed in two steps using the steepest descent algorithm until reaching machine precision, in a first step without constrains, followed by a final step with all bond lengths constrained. All simulations were initialized in three steps: (i) initially, random velocities were generated from a Maxwell–Boltzmann distribution at 303 K and a 100 ps simulation was performed with the positions of all lipid and probe atoms restrained using a force constant of 1000 kJ nm^{-2} mol^{-1}, followed by (ii) further 100 ps with only the probe atoms restrained (1000 kJ nm^{-2} mol^{-1}) and (iii) a final 50 ps unrestrained simulation.

The equations of motion were integrated with the leapfrog algorithm using a time step of 2 fs, with conformations being saved every 10 ps.

Although the setup used in the original Lipid14 parametrization[125] was followed, we nonetheless checked the integrity and fluidity of the bilayer system by running 5 replicates (5x100 ns sampling time after equilibration) of a hydrated POPC bilayer without probes. The obtained average area per lipid of 63.85 ± 0.03 Å is in agreement with the experimental value (64.3 Å),[135] thus showing that the simulated setup provides a proper model of a fluid bilayer, as shown before.[125]

Analysis

The lipid–probe intermolecular interactions (XBs or HBs) were analyzed using a criterion based on a Boltzmann-weighted free energy landscape constructed using the X$\cdots$A distances and C–X$\cdots$A angles (A = XB acceptor), considering the 5 shortest interactions. A similar methodology was used to analyze HB interactions with *iphen*, in this case, by computing O$\cdots$A distances and O–H$\cdots$A angles. All 8 headgroup oxygen atoms (see Figures 1a and S1b) from the 128 phospholipid molecules in the system were considered as potential and independent acceptors. This set of coordinates, which allows for a proper analysis of the XB configurational space,[76] was employed to estimate probability density functions using a Gaussian kernel,[136] and the resulting probability densities were converted into free energies:

$$E(\mathbf{r}) = -RT \ln \frac{P(\mathbf{r})}{P_{\max}} \tag{1}$$

where $\mathbf{r}$ is the coordinate along the 2D space and $P_{\max}$ is the maximum value of the probability density function, $P(\mathbf{r})$.[137] Using these free energy landscapes, XBs were assigned by taking the population of the XB *basin*, i.e., the XB probability for each system and acceptor type was evaluated by calculating the relative population of points that fall into the XB minimum following a steepest-descent path (see Results and Discussion). Concerning the

non-equilibrium segments of the trajectories, the existence of XBs (or HBs) along the simulation time was monitored by mapping the points into the respective (system/ acceptor type) free energy surface.

The probe distribution across the bilayer normal, or membrane insertion along the simulation time, was determined as the z distance between the halogen (or oxygen in the case of *iphen*), or the center-of-mass (COM) of the probe and the average z-position of all phosphorus atoms in the nearest leaflet.

All reported error bars correspond to the standard error of the mean between the 10 independent replicates. Rendered structures were obtained with PyMOL.[138]

Results and Discussion

The potential role of XBs in lipid–ligand interactions was investigated using biomolecular simulations. The configurational space was analyzed with respect to the relative XB sampling involving different acceptor types (CO and PO) from lipid headgroups, differing in their positioning across the bilayer normal and their relative strength as potential XB acceptors (Figure 1a,b). For that purpose several XB donors, consisting of halobenzene probes, were used (Figure 1c). In the case of *iphen*, the presence of competing interactions, i.e. hydrogen bonds (HBs), was also evaluated. In addition, the non-equilibrium insertion events sampled in the simulations were also analyzed, providing evidence for a ubiquitous role for XB interactions in (halo)molecule permeation across biological membranes. For these studies, establishing robust criteria for XB assignment is paramount and therefore, this step will be succinctly discussed in the next Section.

XB Sampling and Assignment Criteria

XB interactions in molecular structures are often evaluated using geometrical criteria,[76] i.e. a C–X$\cdots$A angle larger than 140° and a X$\cdots$A distance shorter than the sum of the

respective van der Waals radii, in agreement with the values typically employed in crystallographic studies or database surveys.[44,65,139,140] This type of approach, however, has a few shortcomings which will be exemplified using ibz^{EP} simulations and CO-type oxygen acceptors. The configurational space can be represented as a free energy surface using $X\cdots A$ distances and $C-X\cdots A$ angles (Figure 2a) and in this system, a free energy minimum is observed within the typical XB region (i.e. $I\cdots O < 3.5$ Å and $C-I\cdots O > 140°$). If a strict geometrical criteria (dash-limited region in Figure 2a) is used, all conformations highlighted in Figure 2b (violet dots) are assigned as XBs. These include many high-energy interactions featuring large deviations from linearity (i.e. very distorted conformations, Figure S10), leading to false-positive XB assignments, while simultaneously not accounting for more elongated sampled interactions that lead to the minimum centered at the XB region. Using a plain geometrical criterion also leads to an erroneous assignment of XBs (i.e. false positives) from simulations without an EP, where the XB region is marginally sampled but without the presence of a XB minimum (data not shown).

To solve this issue, the presence of phospholipid–halobenzene XB interactions was evaluated using the population of the XB *basin*. Taking the Boltzmann-weighted free energy landscape (Figure 2a), the configurations that fall into the XB minimum when following a steepest-descent path are assigned as XBs (Figure 2c, yellow and green). With this approach, the more distorted interactions that would otherwise be assigned as XBs according to plain geometrical criteria (Figure 2c, violet) are replaced by the more elongated interactions (Figure S10) effectively corresponding to XBs in the MM/MD simulations as noted above (Figure 2c, green) that otherwise would be excluded. This strategy also eliminates the aforementioned false positives when running simulations without an EP as no free energy minimum corresponding to XBs is found in the free energy surfaces of those systems (data not shown).
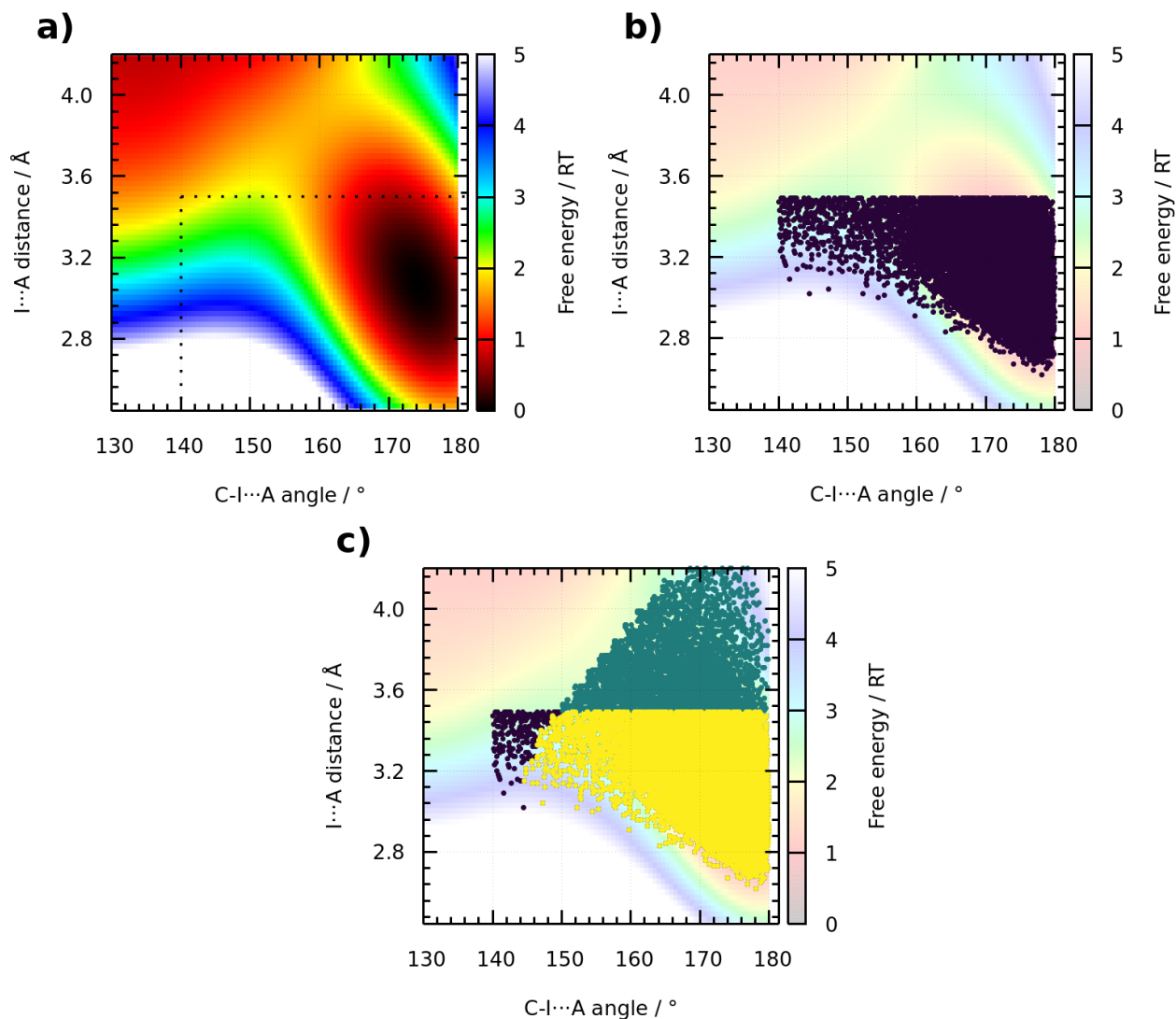
Figure 2: XB sampling according to geometrical criterion or to the population of the XB *basin* illustrated for CO acceptors in *ibz*^{EP} simulations. (a) Free energy surface computed using I···A distances and C–I···A angles. The dash-limited region identifies typical XBs according to geometrical criterion; (b) XBs assigned by applying the geometrical criterion (in violet); (c) XBs assigned using the population of the *basin* criterion (yellow and green) and overlap with the geometrical criteria (in yellow).

XBs in Membrane–Ligand Interactions

As shown in the previous section, a proper criterion to assign XBs relies on the representation of the configurational space as free energy surfaces using X···A distances and C–X···A angles as coordinates, and selecting the configurations that belong to the XB min-

imum, if existent. The landscapes obtained are represented in Figure 3 for the iodinated systems and in Figures S11-S12 for the remainder ones. Apart from the chlorinated systems
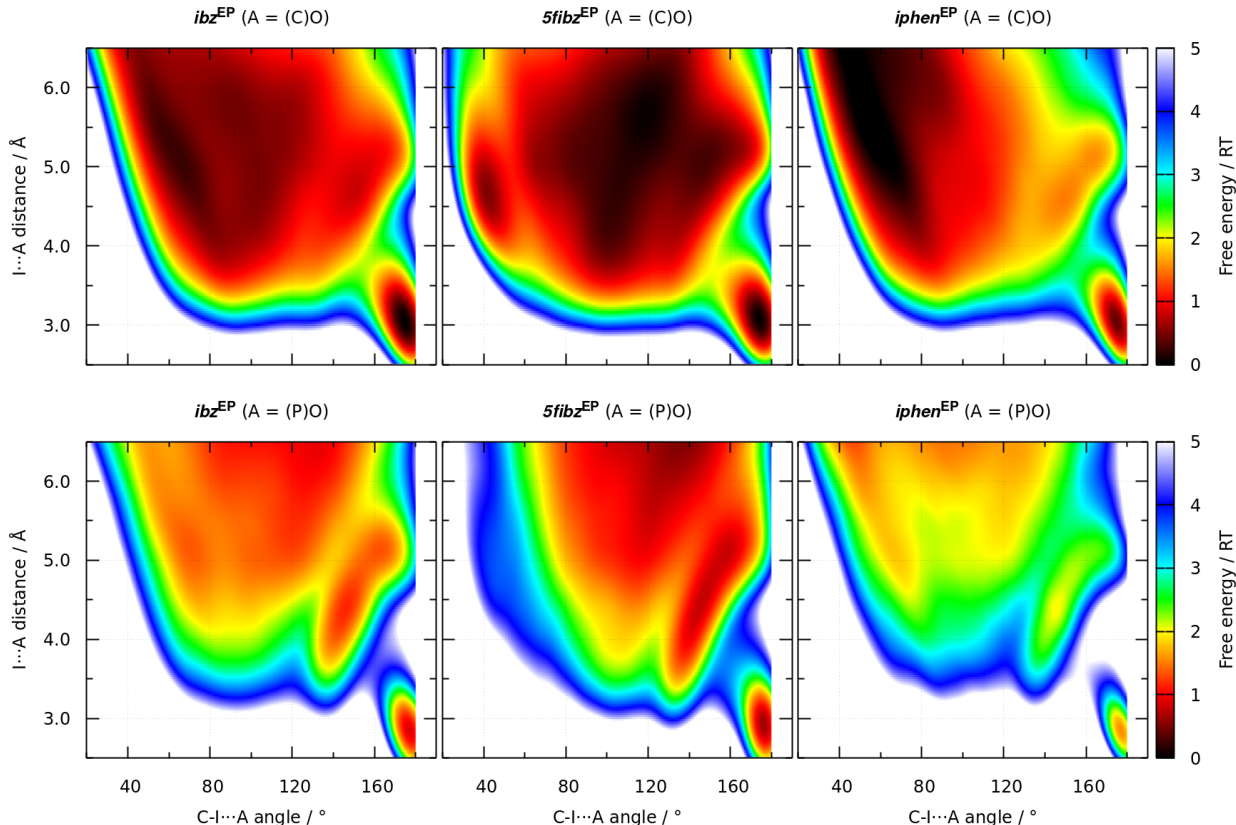

Figure 3: Free energy surfaces using the I···A distances and C–I···A angles for all simulations using iodinated probes. All surfaces are normalized taking as zero the lowest free energy value at the XB region in all simulations (ibz^{EP}).

(cbz^{EP}, $5fcbz^{\mathrm{EP}}$), a minimum on the XB region was obtained for at least one acceptor type thus allowing to evaluate the probability of X···O interactions that effectively correspond to XBs (relative population of the *basin*) for each system and acceptor type (Figure 4). The results provide remarkable evidence for the formation of phospholipid–halobenzene XBs. The total probability can reach a value of c.a. 0.25 in the case of $5fibz^{\mathrm{EP}}$ whereas for ibz^{EP} a similar value is found (0.23). For $iphen^{\mathrm{EP}}$, $5fbbz^{\mathrm{EP}}$, and bbz^{EP} the values drop to 0.12, 0.06, and 0.05, which are still relevant and highlight the potential importance of XBs in mediating membrane–ligand interactions. Figure 5 depicts representative snapshots for such
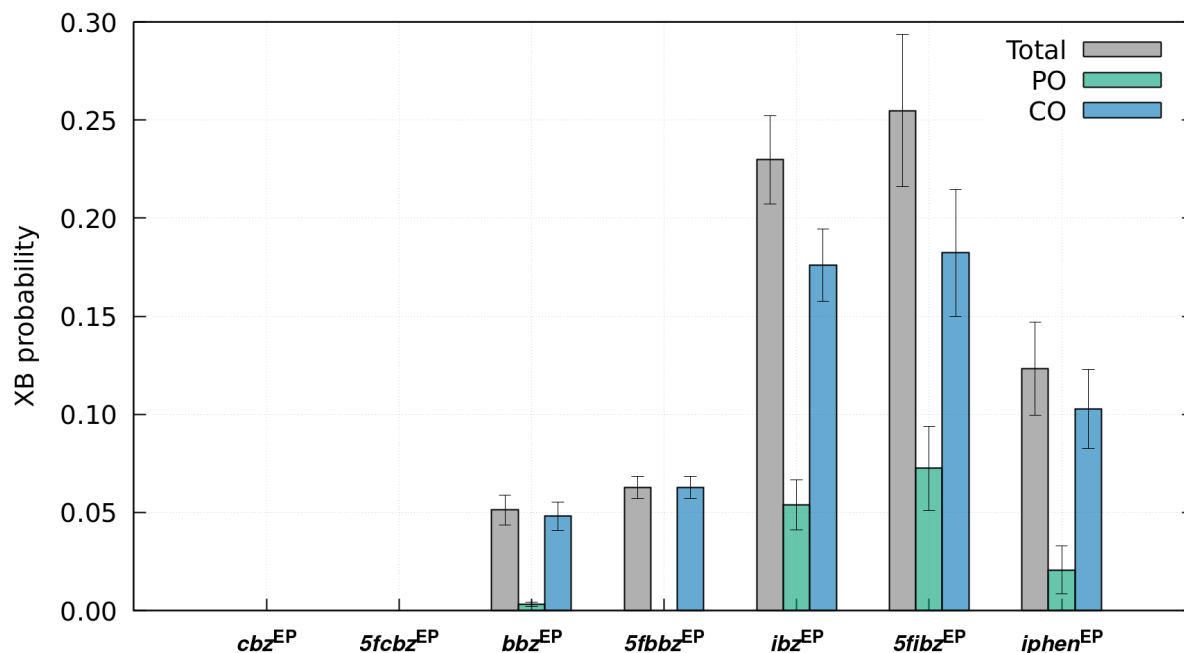
Figure 4: XB probability for all simulated systems.

halogen-bonded conformations involving either PO- or CO-type acceptors, illustrated for $5fibz^{\mathrm{EP}}$ simulations. The calculated probabilities for chlorinated systems are zero as no XB
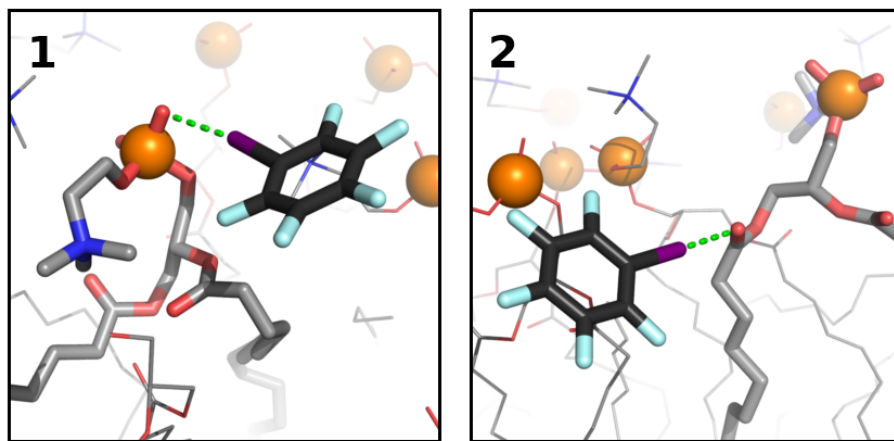

Figure 5: Representative snapshots for halogen-bonded conformations involving either PO-(**1**) or CO-type acceptors (**2**). $5fibz^{\mathrm{EP}}$ and the interacting POPC molecule are shown as sticks with the corresponding XB interactions show as green dashes, phosphorus atoms as spheres, and non-polar hydrogens and water molecules omitted for clarity.

minimum was found.

For each halogen, the total XB probabilities follow the expected order of donor strength based on the V_{max} values, i.e., $C_6F_5X > C_6H_5X$, apart from *iphen* in the iodine series where the lower XB probability is expected given that this molecule is capable of establishing also competing HB interactions (see Section XBs *vs.* HBs in Phospholipid–Halobenzene Recognition below). It should be mentioned however that the difference between the total XB probabilities obtained for the perfluorinated probes *vs.* their hydrogenated counterparts is not as large as expected in light of the significantly stronger XB-donor character of the former.

For all systems showing lipid–ligand XB interactions, the XB probabilities with PO-type acceptors are significantly lower than those observed for CO-type acceptors, contrasting with the expected XB-acceptor strengths (Figure 4). This effect is particularly striking for bromobenzenes where CO acceptors are responsible for all the interactions, XBs with PO being negligible or zero. It should also be added that simultaneous XB interactions involving different acceptor types (i.e. "bifurcated" interactions with both PO- and CO-type acceptors) are not sampled in the simulations, even though numerous neighboring acceptors may be available for interacting in a highly dynamic bilayer environment.

These trends can be rationalized by considering not only the relative XB donor or acceptor strengths, but also the fact that halobenzene molecules, owing to their intrinsically hydrophobic character (log K_{OW} values in the 2.77–3.54 range, see Methods), preferentially populate the inner (ester) region of the membrane more favorably (Figure S13) with the probability peak for the insertion of chlorinated and brominated molecules occurring at larger depths (typically $\geqslant 1$ nm) than their iodinated counterparts (typically < 1 nm). Therefore, the potentially stronger phosphate acceptors are less accessible for establishing XBs. Additionally, the phosphate region is more water exposed whereas the less polar ester region has a stabilizing effect on electrostatically-driven interactions. This is in agreement with the negligible or zero XB probabilities involving PO-acceptors calculated for brominated species.

This analysis can be complemented by also checking the ligand orientation along the membrane normal during the simulations. For that purpose, free energy surfaces using the C–X angle with the bilayer normal, and the halogen insertion along the bilayer, were obtained for iodinated (Figure 6a) and brominated (Figure 7a) systems. Additionally, the probability of
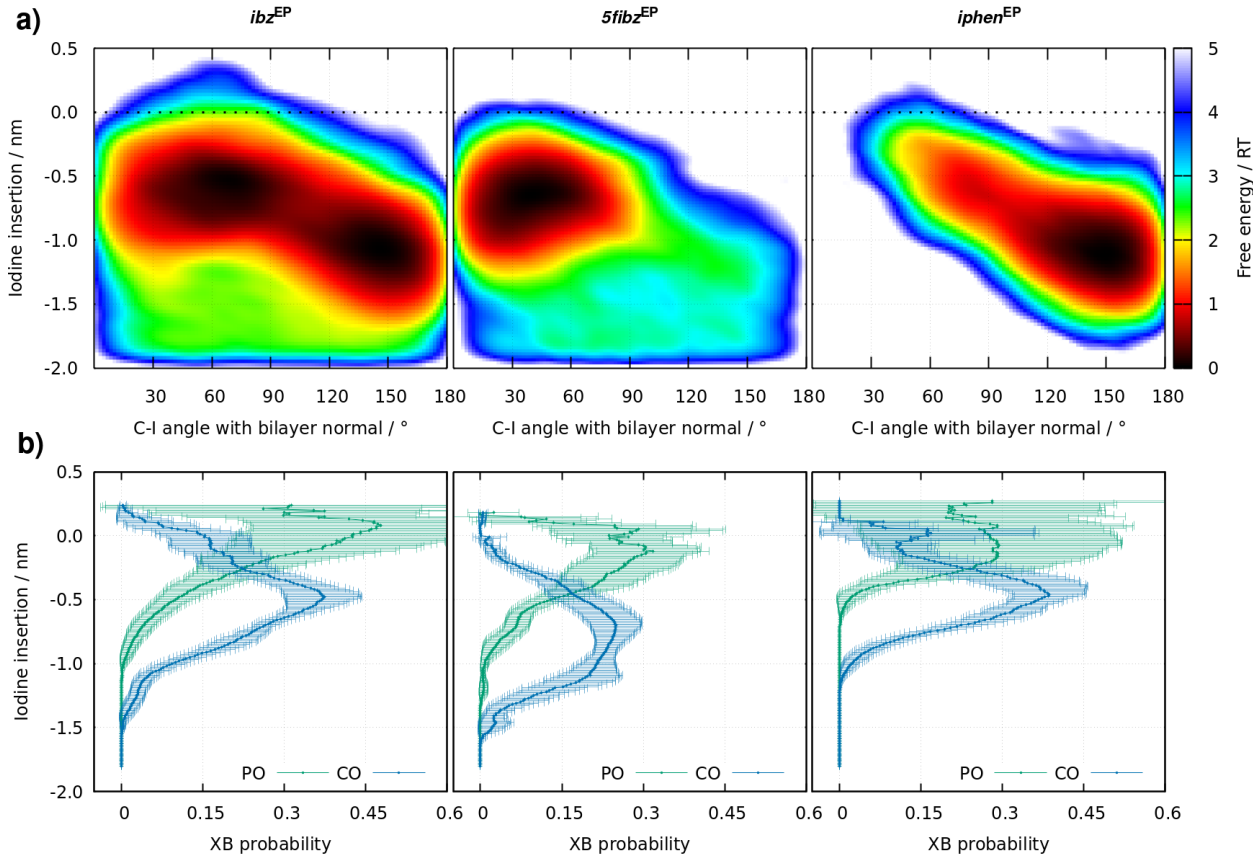

Figure 6: (a) Free energy surfaces using the C–I angle with the bilayer normal and iodine insertion along the bilayer normal. The dashed line corresponds to the average z-position of all phosphorus atoms in the nearest leaflet. (b) XB probability as a function of iodine insertion along the membrane normal.

finding an XB as a function of halogen insertion along the membrane is shown in Figures 6b and 7b for iodinated and brominated systems, respectively.

The $5fibz^{\mathrm{EP}}$ simulations exhibit a single localized free energy minimum at low iodine insertions, centered at c.a. -0.6 nm (corresponding to high XB probabilities) and the C–I vector oriented towards the water phase ($\sim 30°$). In the case of ibz^{EP}, two well-defined
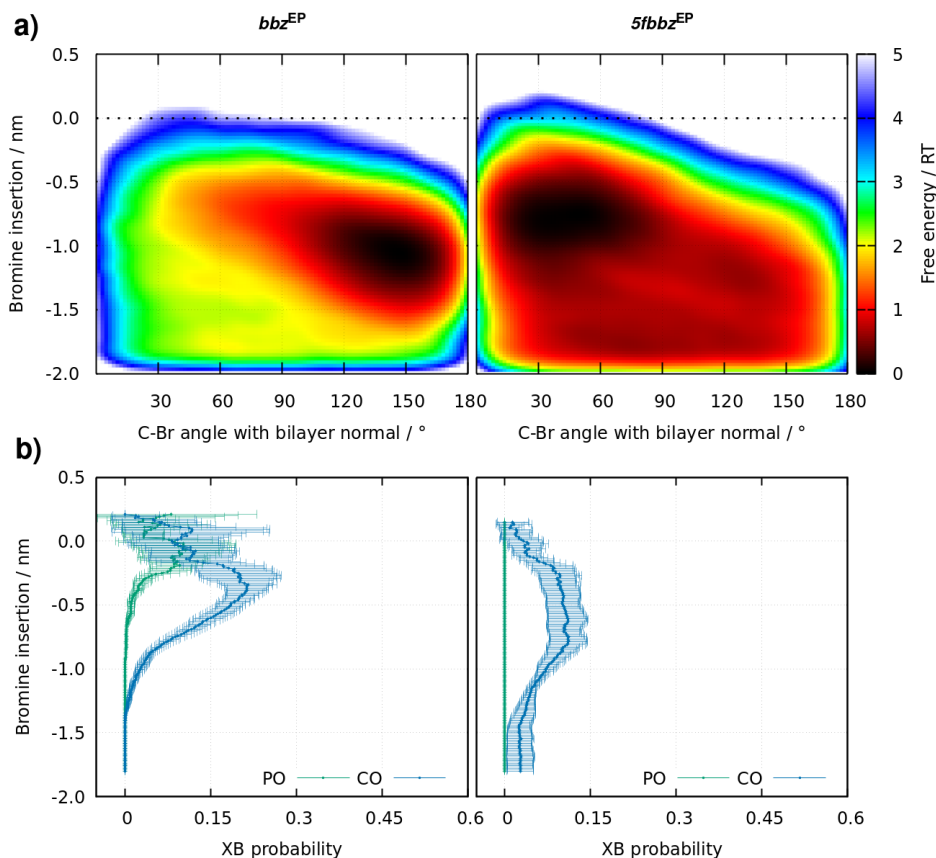
18

Figure 7: (a) Free energy surfaces using the C–Br angle with the bilayer normal and bromine insertion along the bilayer normal. The dashed line corresponds to the average z-position of all phosphorus atoms in the nearest leaflet. (b) XB probability as a function of bromine insertion along the membrane normal.

preferences are observed, one similar to the observed for $5fibz^{\mathrm{EP}}$ but broader and centered at larger angles ($\sim 60°$), and another at higher iodine insertions and with the C–I vector oriented towards the center of the bilayer. At this deeper insertion values, the XB probability is negligible (Figure 6b) as lipid oxygen acceptors are mostly not accessible to engage as interaction partners, and therefore should not account for XB preferences. However, the former minimum indicates a larger rotational variability when compared with $5fibz^{\mathrm{EP}}$, as the molecule may reach C–I angles with the bilayer up to $\sim 90°$ and consequently establish XB interactions, mostly with CO-type acceptors, more favorably. $5fibz^{\mathrm{EP}}$, in contrast, is more rotationally restricted, i.e. mostly oriented towards the water phase, therefore having limited

19

access to XB acceptors (particularly CO) and hence also lower XB probability (Figure 6b), even though XBs can occur at higher depths of the membrane ($\geqslant 1$ nm), owing to local deformations of the membrane that are driven by the stronger XB donor character of the molecule.

Regarding $iphen^{\text{EP}}$, there is a clear preference for conformations featuring the iodine atom inserted closer to the lipid tail region and the C–I vector oriented toward the center of the bilayer (Figure 6a), with the C–O(H) vector oriented toward the water phase, as expected (see Figure S14a). At the higher values of insertion, the XB probabilities are negligible (Figure 6b) and the probability of finding an XB decreases faster with membrane insertion when compared with ibz^{EP}. Again, this rather restricted rotational freedom, caused by competing HBs (see next section), accounts for a lower XB probability. The fact that XBs are responsible for the overall different distribution of the halobenzenes along the membrane is promptly illustrated by comparing the probability density for the membrane insertion obtained with and without the addition of the EP for the iodinated molecules (Figure S15). For ibz, the presence of the EP shifts the distribution to lower insertions when compared with simulations without the EP (where XBs are not sampled, data not shown). This effect is exacerbated in the case of $5fibz$ as it is a strong XB donor, thus supporting that XB interactions indeed impact the membrane insertion preferences of halobenzene ligands. For $iphen$, although a slight deviation is found, the potential effect of the XBs is dominated by the presence of the -OH group that engages in hydrogen bonds and locks the orientation of the molecule and hence its membrane insertion profile.

The behavior of the brominated compounds is rather different. For instance, $5fbbz^{\text{EP}}$ is not rotationally locked when compared to its iodinated counterpart (Figure 7a) and can adopt a wide range of favorable (< 2 RT) membrane insertions and orientations. Hence, the XB probability (CO-type) along the insertion (Figure 7b) decreases less markedly and XBs can be found until very deep membrane insertions. For bbz^{EP}, a well-defined minimum with the C–Br vector oriented towards the lipid tails and larger insertions is observed and,

consequently, the XB probabilities decay very fast with membrane insertion, similarly to what was observed for $iphen^{\mathrm{EP}}$.

As mentioned above, the calculated XB probabilities for chlorinated systems are zero (Figure 4) as no XB minimum is found on the free energy surfaces (Figure S11), despite that region being sampled in our simulations, which is in agreement with chlorine indeed being the weakest XB donor and also with our preliminary QM calculations on model systems (Table S1) for which halogen-bonded minima could not be located. While perfluorination increases the σ–hole, a concomitant increase in membrane insertion is also observed (Figures S13 and S16) in line with the increase of the log K_{OW} values (2.77 to 3.18). Altogether, our results show that despite perfluorination being often used as a strategy to increase membrane permeability, in the case of the more polarizable iodobenzene derivatives this may lead to a dramatic increase in the XB donor properties causing the iodine atom of $5fibz^{\mathrm{EP}}$ to populate the inner region of the membrane less favorably (smaller insertions) than ibz^{EP}. In contrast, for brominated and chlorinated systems perfluorination leads to higher halogen-atom insertions (Figure S13) resulting in low to non-existent XBs. Notwithstanding, these results do not preclude the existence of membrane–ligand XBs in other chlorinated systems where the delicate balance between the σ–hole magnitude and lipophilicity can be tuned.

XBs *vs.* HBs in Phospholipid–Halobenzene Recognition

4-Iodophenol exhibits both halogen- and hydrogen-bonding donors, rendering it a suitable model to study the eventual competing effect of the two types of intermolecular interactions that may occur in complex, multi-functionalized drug-like compounds. As previously shown, XBs are less favored for $iphen^{\mathrm{EP}}$ when compared with the remainder iodinated systems (Figure 4), a result that may be driven by the capability of $iphen$ to establish competing HB interactions.

To evaluate this, the same approach developed for XB was followed, in this case, by taking the configurations belonging to the HB *basin* on a $O \cdots A$ distance, O–$H \cdots A$ angle

free energy landscape and computing the HB probability (Figure S17). As expected, the two types of HB interactions involving phosphate- (PO) or ester- (CO) type oxygen acceptors (**1** and **2**, respectively, in Figure 8) are sampled and, as for XBs, HB interactions targeting simultaneously the two acceptor types do no occur. The relative probability of HBs and
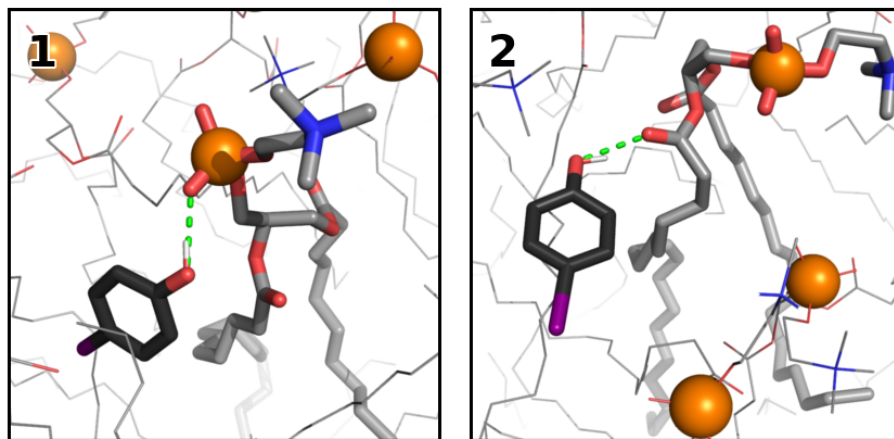

Figure 8: Representative snapshots for hydrogen-bonded conformations involving either PO- (**1**) or CO-type (**2**) acceptors. HB interactions are shown as green dashes (coloring scheme as in Figure 5).

XBs (Figure S17) shows that HBs (c.a. 0.23) are preferred over XB interactions (c.a. 0.12) and the same interaction preference for CO-type acceptors is observed for both interactions. However, the probability of HBs targeting PO-type acceptors is larger than that found for XBs, in agreement with the observed preference for deeper iodine insertions (Figure 6a) and more shallow OH insertions (Figure S14a). Also, HB probability increases at outer regions of the membrane for PO-type acceptors (Figure S14b), however, HBs can still be sampled for CO-type acceptors at inner membrane regions owing to the stronger nature of the interactions which may stabilize the presence of more membrane-inserted lipid headgroups in the simulations.

The eventual occurrence of the two types of interactions (HBs and XBs) simultaneously was also analyzed allowing to infer if the reported probabilities pertain to exclusively hydrogen- (or halogen-) bonded to conformations or, alternatively, if the two interactions

may stabilize phospholipid–*iphen* binding simultaneously. Indeed, simultaneous XB and HB interactions are observed, leading to "XHB"-like structures (Figure 9) that account for only c.a. 0.03 of the interactions. These configurations correspond, for example, to two simultaneous XB and HB interactions with ester oxygen (CO)-type acceptors from different phospholipid molecules (**1**, Figure 9) which is the most representative type of XHB interactions observed in the simulations (c.a. 0.015). Apart from simultaneous XBs and HBs with PO-type acceptors which are negligible (c.a. 0.0001, **4** in Figure 9), all the other combinations of XHB interactions are observed, including less favorable structures featuring a CO-type XB and a PO-type HB (c.a. 0.0083), or a PO-type XB together with a CO-type HB (c.a. 0.0055), simultaneously (Figure 9, **2** and **3**, respectively). In spite of XHB interactions being scarcely sampled (c.a. 0.03), these results show that XB and HB interactions may not only compete towards the same lipid acceptor but also act cooperatively via two simultaneous bonds with different acceptors in phospholipid–halobenzene recognition phenomena.

Membrane Insertion Process

In the previous sections we have shown that, in equilibrium, halobenzene probes can interact favorably with phospholipids via XBs (and HBs) with both phosphate (PO)- and ester (CO)-type lipid oxygen acceptors. In this section, we discuss a potential role for halogen bonding in the membrane-internalization process, i.e. water/membrane interface crossing, by analyzing the non-equilibrium segments of the simulations corresponding to the membrane insertion events sampled in the simulations starting with the halobenzenes in the water phase. The halogen insertion along the membrane normal was monitored while simultaneously evaluating the presence of XB (and HB) interactions. We were able to distinguish between "on" (interacting) and "off" (non-interacting) states during the insertion process. Figure 10 illustrates the process for representative simulations for all systems featuring iodinated and brominated probes (see Figures S18-S22 for all insertion events). Chlorinated probes were not considered as no XBs were observed in the equilibrium simulations. Haloben-
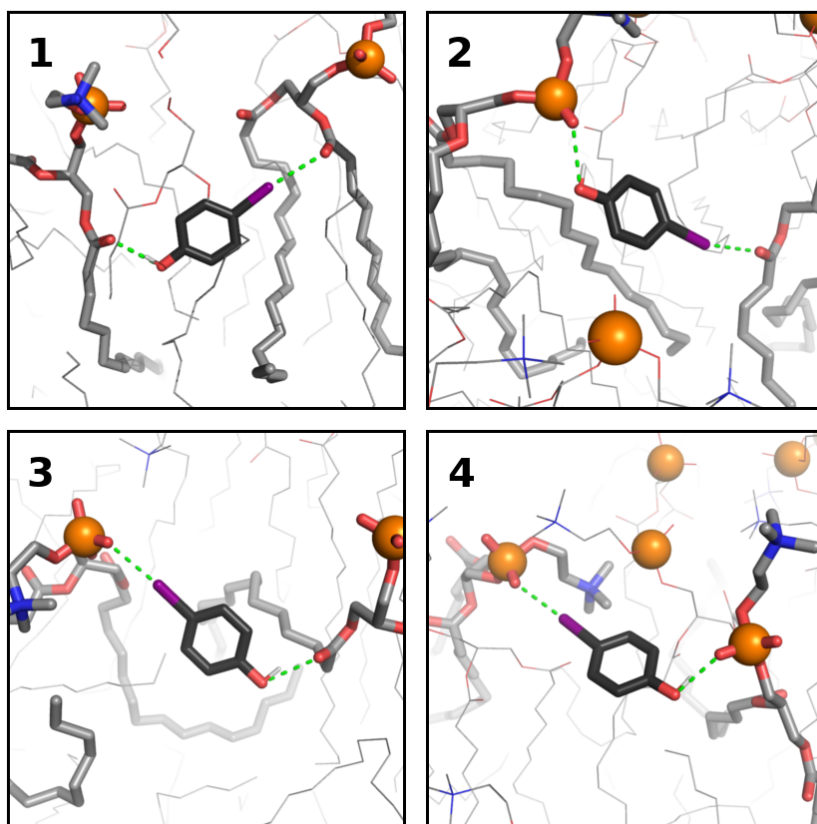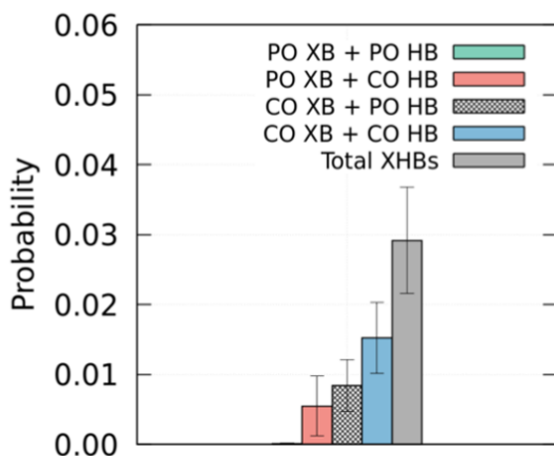
Figure 9: XHB probability for the *iphen*[EP] simulations along with representative snapshots for each type of XHB interaction (coloring scheme as in Figure 5).

zene insertion processes typically occurs in short time-scales (< 6 ns), with the exception of a few replicates, and XB interactions are frequently sampled preceding the membrane internalization events, i.e. with the halobenzene in the water phase, typically involving the
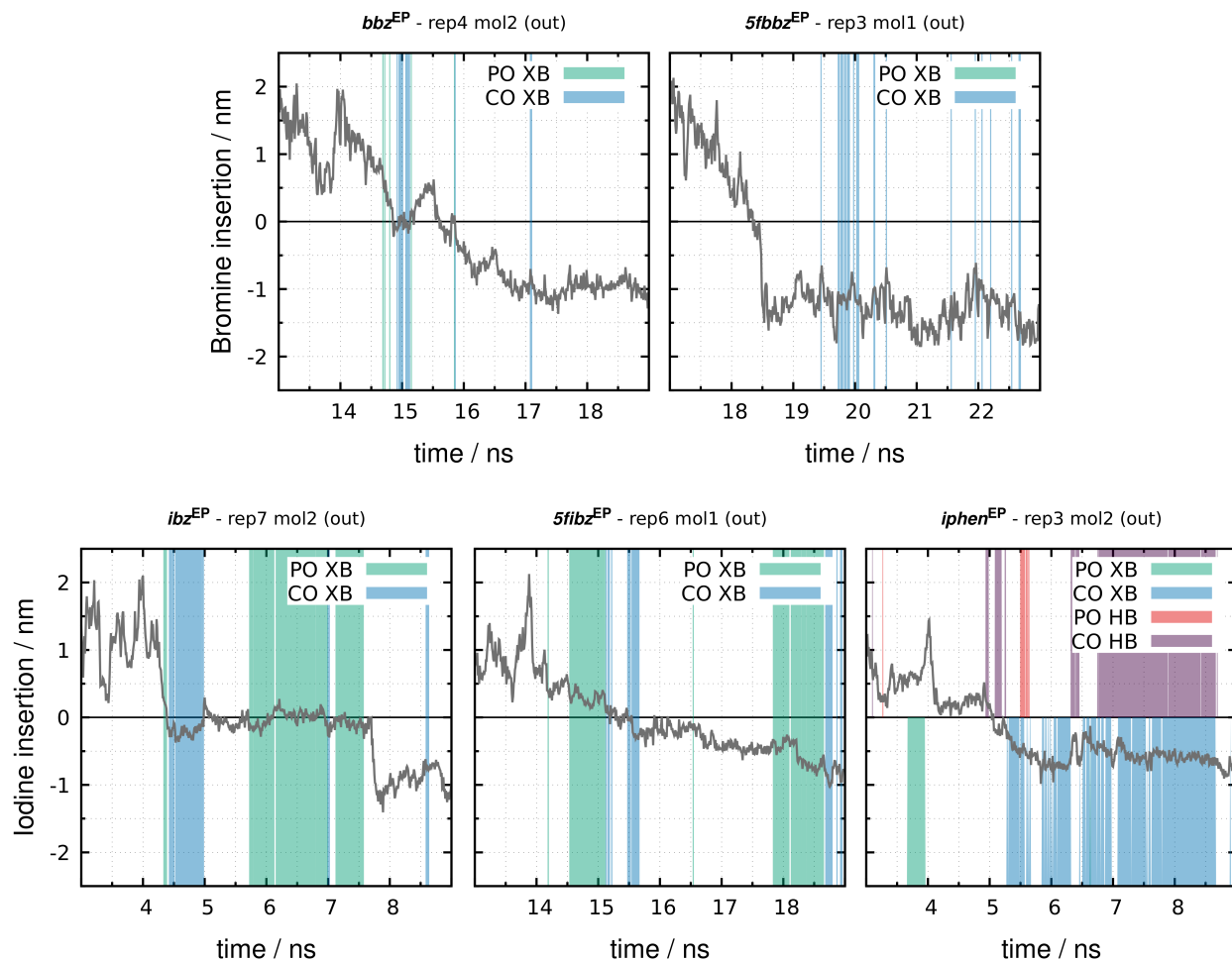
Figure 10: Halogen insertion process for a representative replicate of each system for iodinated and brominated probes. The solid horizontal line corresponds to the average z-position of all phosphorus atoms in the nearest leaflet. The presence of XBs or HBs ("on" states) is depicted as vertical lines.

more water-exposed PO-type acceptors (shown in green) though examples of interactions with CO-type (in blue) acceptors were also identified. Interestingly, XB interactions are systematically observed during all insertion events sampled in the simulations, as shown in Figures 10 and S18-S22. These events are characterized by different types of interaction patterns for each replicate / system, though a prevalence of a mechanism involving PO-type interaction(s) followed by CO-type interaction(s), as shown in Figure 10, is observed, while other mechanisms, e.g. involving only CO-type interactions, also occur. In the specific

case of $5fbbz^{\mathrm{EP}}$ simulations only CO-type interactions are observed upon insertion, in agreement with the observed absence of XBs with PO-type acceptors in equilibrium simulations. Furthermore, XB interactions may either exhibit short kinetics or take place in extended time-scales, depending on the system / replicate. In the case of $iphen^{\mathrm{EP}}$ simulations, HB interactions are also frequently established prior to membrane insertion and typically targeting PO-type acceptors (shown in red, Figure S22), however, XBs are also often observed. Indeed, the two types of interactions are systematically present during the internalization process with their relative interplay determining different interaction patterns (Figure S22). This qualitative analysis of non-equilibrium insertion events provides seminal evidence that XB interactions may play a role in mediating the permeation of halogenated small molecules across biological membranes, parallel to the well-known ubiquitous role of hydrogen-bonding in HB-donor molecules.[22–26]

Conclusions

The potential role of halogen bonding in the context of biological membrane systems was poorly understood when compared with the recognized importance of XB interactions in protein–ligand complexes or nucleic acids. Indeed, to the best of our knowledge, no previous literature reports have addressed XB-mediated membrane–ligand recognition phenomena, despite the well-known prevalence of halogenated molecules in drug discovery and development[41–44] and the existence of multiple XB acceptors in phospholipids, the main constituent of a cell membranes. To explore the existence of phospholipid–halogen interactions, we carried out MM/MD simulations with a series of halobenzenes in a hydrated phospholipid (POPC) bilayer environment, using an extra-point (EP) approach to model the XB-properties of the halogenated species.[81–84] This methodology, that had been widely applied in the computational investigation of a variety of protein–ligand systems,[86–89,102,104,105] provided evidences supporting the role of XB interactions in lipid–ligand recognition events.

XB interactions involving both phosphate (PO) and ester (CO) oxygen acceptors were evaluated and assigned from the sampled configurations using a criterion based on a Boltzmann-weighted free energy landscape constructed using $X \cdots A$ distances and the $C–X \cdots A$ angles, selecting the configurations that belong to the XB *basin*. This criterion provides an accurate description of halogen-bonding in the simulations by removing false positives obtained when using a plain geometrical cutoff. The results show that halobenzene derivatives (apart from the chlorinated ones) interact with model phospholipid membranes via XB interactions targeting both PO- and CO-type acceptors, the latter interactions being electrostatically favored due to the less water-exposed environment and intrinsically hydrophobic character ($2.77 < \log K_{OW} < 3.54$) of the probe molecules, despite PO-type acceptors being stronger XB interaction partners. XB probability is also dependent on the orientational preferences with respect to the bilayer normal, with perfluorination favoring higher membrane insertions when XBs are weaker (brominated derivatives), or lower insertions in the case of stronger iodinated molecules together with the C–I vector oriented towards the water phase and hence more limited access to XB acceptors. Nonetheless, the total XB frequencies typically follow the expected order of relative XB donor strength.

Our results also showed that, similarly to other biological systems,[30,80] XBs can compete with HBs in the case of small molecules bearing both XB- and HB-donor moieties such as *iphen*. Even though $O–H \cdots O$ interactions are slightly stronger than the $I \cdots O$ counterparts, the two types of interactions can also occur simultaneously in transient higher free-energy "XHB-like" conformations which may act either cooperatively or competitively in mediating membrane–probe recognition events.

The non-equilibrium segments of the trajectories corresponding to the membrane insertion events sampled in the simulations starting with the molecules in the water phase were analyzed by monitoring the halogen insertion along the membrane normal over time and simultaneously assessing the presence of XB interactions. XBs were observed in all replicates, often preceding internalization, suggesting a potential role in promoting the water-to-

membrane insertion process of halogenated molecules.

In summary, the role of XB interactions in lipid–ligand systems was tackled for the first time and our data provide important insights into membrane–(halo)drug recognition mechanisms at the molecular level. In particular, we propose that biomembrane recognition of drug-like compounds can be directly mediated by XB interactions implying that, beyond often exhibiting superior pharmacokinetic profile, namely enhanced passive membrane diffusion,[45] bioactive halogenated molecules may further reach biological targets via direct phospholipid–halogen interactions, as previously suggested,[70] which may contribute determinedly to their pharmacological efficacy or, on the contrary, to their toxicological effects. This concept opens the possibility for the rational design of novel drugs by taking advantage of lipid–halogen recognition phenomena which is important in the field of membrane-lipid therapy,[3] and can be used as a starting point to design molecules that target specific membrane domains associated with several human diseases. Moreover, these findings can also contribute to the improvement of molecular descriptors for QSAR models aiming at predicting permeability or toxicity as these should account for XB-capability, similarly to the ubiquitous hydrogen bond.[22–26]

Finally, we note that while this work reinforces the usefulness of MM/MD simulations in the study XB-mediated biomembrane recognition phenomena, further investigation of these processes in the context of large datasets of drug-like molecules is envisaged. Moreover, we hope these results will encourage experimental investigation aiming at an improved understanding of phospholipid–halogen interactions at the molecular level.

Supporting Information Available

Supporting Figures (PDF).

Topology files in ITP format for all of the parameterized halobenzene probes (ZIP).

Acknowledgement

References

(1) Imming, P.; Sinning, C.; Meyer, A. Drugs, their targets and the nature and number of drug targets. *Nat. Rev. Drug Discov.* **2006**, *5*, 821.

(2) Yin, H.; Flynn, A. D. Drugging membrane protein interactions. *Annu. Rev. Biomed. Eng.* **2016**, *18*, 51–76.

(3) Escribá, P. V. Membrane-lipid therapy: a new approach in molecular medicine. *Trends Mol. Med.* **2006**, *12*, 34–43.

(4) Ingolfsson, H. I. et al. Phytochemicals perturb membranes and promiscuously alter protein function. *ACS Chem. Biol.* **2014**, *9*, 1788–1798.

(5) Baell, J. B. Screening-Based Translation of Public Research Encounters Painful Problems. *ACS Med. Chem. Lett.* **2015**, *6*, 229–234.

(6) Baell, J. B. Feeling nature's PAINS: natural products, natural product drugs, and pan assay interference compounds (PAINS). *J. Nat. Prod.* **2016**, *79*, 616–628.

(7) Perkins, R.; Vaida, V. Phenylalanine increases membrane permeability. *J. Am. Chem. Soc.* **2017**, *139*, 14388–14391.

(8) Epand, R. M.; Walker, C.; Epand, R. F.; Magarvey, N. A. Molecular mechanisms of membrane targeting antibiotics. *BBA Biomembranes* **2016**, *1858*, 980–987.

(9) Li, J.; Koh, J.-J.; Liu, S.; Lakshminarayanan, R.; Verma, C. S.; Beuerman, R. W. Membrane active antimicrobial peptides: translating mechanistic insights to design. *Front. Neurosci.* **2017**, *11*, 73.

(10) Hurdle, J. G.; O'neill, A. J.; Chopra, I.; Lee, R. E. Targeting bacterial membrane function: an underexploited mechanism for treating persistent infections. *Nat. Rev. Microbiol.* **2011**, *9*, 62–75.

(11) Dias, C. et al. Sugar-based bactericides targeting phosphatidylethanolamine-enriched membranes. *Nat. Commun.* **2018**, *9*, 4857.

(12) Dias, C.; Rauter, A. P. Membrane-targeting antibiotics: recent developments outside the peptide space. *Future Med. Chem.* **2019**, *11*, 211–228.

(13) Hendrich, A.; Michalak, K. Lipids as a target for drugs modulating multidrug resistance of cancer cells. *Curr. Drug Targets* **2003**, *4*, 23–30.

(14) Sharom, F. J.; Mellors, A. Effects of polychlorinated biphenyls on biological membranes: Physical toxicity and molar volume relationships. *Biochem. Pharmacol.* **1980**, *29*, 3311–3317.

(15) Ogunbayo, O. A.; Jensen, K. T.; Michelangeli, F. The interaction of the brominated flame retardant: tetrabromobisphenol A with phospholipid membranes. *BBA Biomembranes* **2007**, *1768*, 1559–1566.

(16) Tan, Y.; Chen, C.-H.; Lawrence, D.; Carpenter, D. O. Ortho-substituted PCBs kill cells by altering membrane structure. *Toxicol. Sci.* **2004**, *80*, 54–59.

(17) Lipinski, C. A. Avoiding investment in doomed drugs. *Curr. Drug. Discov.* **2001**, *1*, 17–19.

(18) Matsson, P.; Kihlberg, J. How Big Is Too Big for Cell Permeability? *J. Med. Chem.* **2017**, *60*, 1662–1664.

(19) Waring, M. J. Lipophilicity in drug discovery. *Exp. Opin. Drug Discov.* **2010**, *5*, 235–248.

(20) Yue, Z.; Li, C.; Voth, G. A.; Swanson, J. M. Dynamic Protonation Dramatically Affects the Membrane Permeability of Drug-like Molecules. *J. Am. Chem. Soc.* **2019**, *141*, 13421–13433.

(21) Dickson, C. J.; Hornak, V.; Bednarczyk, D.; Duca, J. S. Using membrane partitioning simulations to predict permeability of forty-nine drug-like molecules. *J. Chem. Inf. Model.* **2019**, *59*, 236–244.

(22) Lipinski, C. A.; Lombardo, F.; Dominy, B. W.; Feeney, P. J. Experimental and computational approaches to estimate solubility and permeability in drug discovery and development settings. *Adv. Drug Deliv. Rev.* **2001**, *46*, 3–26.

(23) Bemporad, D.; Luttmann, C.; Essex, J. Behaviour of small solutes and large drugs in a lipid bilayer from computer simulations. *BBA Biomembranes* **2005**, *1718*, 1–21.

(24) Shinoda, W. Permeability across lipid membranes. *BBA Biomembranes* **2016**, *1858*, 2254–2265.

(25) Dickson, C. J.; Hornak, V.; Pearlstein, R. A.; Duca, J. S. Structure–kinetic relationships of passive membrane permeation from multiscale modeling. *J. Am. Chem. Soc.* **2017**, *139*, 442–452.

(26) Rezai, T.; Bock, J. E.; Zhou, M. V.; Kalyanaraman, C.; Lokey, R. S.; Jacobson, M. P. Conformational flexibility, internal hydrogen bonding, and passive membrane permeability: successful in silico prediction of the relative permeabilities of cyclic peptides. *J. Am. Chem. Soc.* **2006**, *128*, 14073–14080.

(27) Desiraju, G. R.; Ho, P. S.; Kloo, L.; Legon, A. C.; Marquardt, R.; Metrangolo, P.; Politzer, P.; Resnati, G.; Rissanen, K. Definition of the halogen bond (IUPAC Recommendations 2013). *Pure Appl. Chem.* **2013**, *85*, 1711–1713.

(28) Clark, T.; Hennemann, M.; Murray, J. S.; Politzer, P. Halogen bonding: the σ-hole. *J. Mol. Model.* **2007**, *13*, 291–296.

(29) Cavallo, G.; Metrangolo, P.; Milani, R.; Pilati, T.; Priimagi, A.; Resnati, G.; Terraneo, G. The halogen bond. *Chem. Rev.* **2016**, *116*, 2478–2601.

(30) Costa, P. J. The halogen bond: nature and applications. *Phys. Sci. Rev.* **2017**, *2*, 20170136.

(31) Auffinger, P.; Hays, F. A.; Westhof, E.; Ho, P. S. Halogen bonds in biological molecules. *Proc. Natl. Acad. Sci. USA* **2004**, *101*, 16789–16794.

(32) Parisini, E.; Metrangolo, P.; Pilati, T.; Resnati, G.; Terraneo, G. Halogen bonding in halocarbon–protein complexes: a structural survey. *Chem. Soc. Rev.* **2011**, *40*, 2267–2278.

(33) Scholfield, M. R.; Zanden, C. M. V.; Carter, M.; Ho, P. S. Halogen bonding (X-bonding): a biological perspective. *Protein Sci.* **2013**, *22*, 139–152.

(34) Voth, A. R.; Hays, F. A.; Ho, P. S. Directing macromolecular conformation through halogen bonds. *Proc. Natl. Acad. Sci. USA* **2007**, *104*, 6188–6193.

(35) Parker, A. J.; Stewart, J.; Donald, K. J.; Parish, C. A. Halogen bonding in DNA base pairs. *J. Am. Chem. Soc.* **2012**, *134*, 5165–5172.

(36) Carter, M.; Voth, A. R.; Scholfield, M. R.; Rummel, B.; Sowers, L. C.; Ho, P. S. Enthalpy–entropy compensation in biomolecular halogen bonds measured in DNA junctions. *Biochemistry* **2013**, *52*, 4891–4903.

(37) Ford, M. C.; Saxton, M.; Ho, P. S. Sulfur as an acceptor to bromine in biomolecular halogen bonds. *J. Phys. Chem. Lett.* **2017**, *8*, 4246–4252.

(38) Kolář, M. H.; Tabarrini, O. Halogen Bonding in Nucleic Acid Complexes: Miniperspective. *J. Med. Chem.* **2017**, *60*, 8681–8690.

(39) Frontera, A.; Bauza, A. Halogen bonds in protein nucleic acid recognition. *J. Chem. Theory Comput.* **2020**, *16*, 4744–4752.

(40) Piña, M. d. l. N.; Frontera, A.; Bauza, A. Quantifying intramolecular Halogen Bonds in Nucleic Acids: A combined PDB and theoretical study. *ACS Chem. Biol.* **2020**, *15*, 1942–1948.

(41) Ho, P. S. Halogen bonding in medicinal chemistry: from observation to prediction. *Future Med. Chem.* **2017**, *9*, 637–640.

(42) Wilcken, R.; Zimmermann, M. O.; Lange, A.; Joerger, A. C.; Boeckler, F. M. Principles and applications of halogen bonding in medicinal chemistry and chemical biology. *J. Med. Chem.* **2013**, *56*, 1363–1388.

(43) Costa, P. J.; Nunes, R.; Vila-Viçosa, D. Halogen bonding in halocarbon-protein complexes and computational tools for rational drug design. *Expert Opin. Drug Discov.* **2019**, *14*, 805–820.

(44) Xu, Z.; Yang, Z.; Liu, Y.; Lu, Y.; Chen, K.; Zhu, W. Halogen bond: its role beyond drug–target binding affinity for drug discovery and development. *J. Chem. Inf. Model.* **2014**, *54*, 69–78.

(45) Gerebtzoff, G.; Li-Blatter, X.; Fischer, H.; Frentzel, A.; Seelig, A. Halogenation of drugs enhances membrane binding and permeation. *ChemBioChem* **2004**, *5*, 676–684.

(46) Ungati, H.; Govindaraj, V.; Mugesh, G. The Remarkable Effect of Halogen Substitution on the Membrane Transport of Fluorescent Molecules in Living Cells. *Angew. Chem. Int. Ed.* **2018**, *57*, 8989–8993.

(47) Ungati, H.; Govindaraj, V.; Nair, C. R.; Mugesh, G. Halogen-Mediated Membrane Transport: An Efficient Strategy for the Enhancement of Cellular Uptake of Synthetic Molecules. *Chem. Eur. J.* **2019**, *25*, 3391–3399.

(48) Jakka, S. R.; Govindaraj, V.; Mugesh, G. A Single Atom Change Facilitates the Membrane Transport of Green Fluorescent Proteins in Mammalian Cells. *Angew. Chem. Int. Ed.* **2019**, *58*, 7713–7717.

(49) Govindaraj, V.; Ungati, H.; Jakka, S. R.; Bose, S.; Mugesh, G. Directing Traffic: Halogen bond-mediated Membrane Transport. *Chem. Eur. J.* **2019**, *25*, 11180–11192.

(50) Wang, T.; Yin, P.; Yang, Y.; Yin, W.; Zhang, S.; Yang, M.; Qin, Y.; Ma, Y.; Lei, Z.; Ma, H. Effect of Element Iodine on the Cell Membrane Transportability of Fluorescent Polymers and Lysosome-Targeted Cell Imaging. *ACS Sustainable Chem. Eng.* **2019**, *7*, 6295–6303.

(51) Rashid, A.; Vakurov, A.; Mohamadi, S.; Sanver, D.; Nelson, A. Substituents modulate biphenyl penetration into lipid membranes. *BBA Biomembranes* **2017**, *1859*, 712–721.

(52) Beale, T. M.; Chudzinski, M. G.; Sarwar, M. G.; Taylor, M. S. Halogen bonding in solution: thermodynamics and applications. *Chem. Soc. Rev.* **2013**, *42*, 1667–1680.

(53) Zapata, F.; Caballero, A.; White, N. G.; Claridge, T. D. W.; Costa, P. J.; Félix, V.; Beer, P. D. Fluorescent charge-assisted halogen-bonding macrocyclic halo-imidazolium receptors for anion recognition and sensing in aqueous media. *J. Am. Chem. Soc.* **2012**, *134*, 11533–11541.

(54) Langton, M. J.; Robinson, S. W.; Marques, I.; Félix, V.; Beer, P. D. Halogen bonding in water results in enhanced anion recognition in acyclic and rotaxane hosts. *Nat. Chem.* **2014**, *6*, 1039–1043.

(55) Jentzsch, A. V.; Emery, D.; Mareda, J.; Nayak, S. K.; Metrangolo, P.; Resnati, G.; Sakai, N.; Matile, S. Transmembrane anion transport mediated by halogen-bond donors. *Nat. Commun.* **2012**, *3*, 905.

(56) Vargas Jentzsch, A.; Matile, S. Transmembrane halogen-bonding cascades. *J. Am. Chem. Soc.* **2013**, *135*, 5302–5303.

(57) Jentzsch, A. V.; Matile, S. Anion Transport with Halogen Bonds. In *Halogen Bonding I: Impact on Materials Chemistry and Life Sciences. Topics in Current Chemistry*; Metrangolo, P., Resnati, G., Eds.; Springer International Publishing: Cham, 2014; Vol. 358; pp 205–239.

(58) Ren, C.; Ding, X.; Roy, A.; Shen, J.; Zhou, S.; Chen, F.; Li, S. F. Y.; Ren, H.; Yang, Y. Y.; Zeng, H. A halogen bond-mediated highly active artificial chloride channel with high anticancer activity. *Chem. Sci.* **2018**, *9*, 4044–4051.

(59) Vargas Jentzsch, A.; Hennig, A.; Mareda, J.; Matile, S. Synthetic ion transporters that work with anion- π interactions, halogen bonds, and anion–macrodipole interactions. *Acc. Chem. Res.* **2013**, *46*, 2791–2800.

(60) Benz, S.; Macchione, M.; Verolet, Q.; Mareda, J.; Sakai, N.; Matile, S. Anion transport with chalcogen bonds. *J. Am. Chem. Soc.* **2016**, *138*, 9093–9096.

(61) Haynes, C. J.; Moore, S. J.; Hiscock, J. R.; Marques, I.; Costa, P. J.; Félix, V.; Gale, P. A. Tunable transmembrane chloride transport by bis-indolylureas. *Chem. Sci.* **2012**, *3*, 1436–1444.

(62) Moore, S. J.; Haynes, C. J.; González, J.; Sutton, J. L.; Brooks, S. J.; Light, M. E.; Herniman, J.; Langley, G. J.; Soto-Cerrato, V.; Pérez-Tomás, R.; Marques, I.; Costa, P. J.; Félix, V.; Gale, P. A. Chloride, carboxylate and carbonate transport by ortho-phenylenediamine-based bisureas. *Chem. Sci.* **2013**, *4*, 103–117.

(63) Marques, I.; Colaço, A. R.; Costa, P. J.; Busschaert, N.; Gale, P. A.; Félix, V. Tris–thiourea tripodal-based molecules as chloride transmembrane transporters: insights from molecular dynamics simulations. *Soft Matter* **2014**, *10*, 3608–3621.

(64) Wilcken, R.; Zimmermann, M. O.; Lange, A.; Zahn, S.; Boeckler, F. M. Using halogen bonds to address the protein backbone: a systematic evaluation. *J. Comput. Aided Mol. Design* **2012**, *26*, 935–945.

(65) Zhang, Q.; Xu, Z.; Shi, J.; Zhu, W. Underestimated halogen bonds forming with protein backbone in protein data bank. *J. Chem. Inf. Model.* **2017**, *57*, 1529–1534.

(66) Chowdhury, B.; Sinha, S.; Ghosh, P. Selective Sensing of Phosphates by a New Bis-heteroleptic RuII Complex through Halogen Bonding: A Superior Sensor over Its Hydrogen-Bonding Analogue. *Chem. Eur. J.* **2016**, *22*, 18051–18059.

(67) Schaub, T. A.; Sure, R.; Hampel, F.; Grimme, S.; Kivala, M. Quantum chemical dissection of the shortest $P=O\cdots I$ halogen bond: the decisive role of crystal packing effects. *Chem. Eur. J.* **2017**, *23*, 5687–5691.

(68) Cabot, R.; Hunter, C. A. Non-covalent interactions between iodo-perfluorocarbons and hydrogen bond acceptors. *Chem. Commun.* **2009**, 2005–2007.

(69) Chudzinski, M. G.; Taylor, M. S. Correlations between computation and experimental thermodynamics of halogen bonding. *J. Org. Chem.* **2012**, *77*, 3483–3491.

(70) Nayak, S. K.; Terraneo, G.; Piacevoli, Q.; Bertolotti, F.; Scilabra, P.; Brown, J. T.;

Rosokha, S. V.; Resnati, G. Molecular Bases for Anesthetic Agents: Halothane as a Halogen-and Hydrogen-Bond Donor. *Angew. Chem. Int. Ed.* **2019**, *58*, 12456–12459.

(71) Xu, Y.; Huang, J.; Gabidullin, B.; Bryce, D. L. A rare example of a phosphine as a halogen bond acceptor. *Chem. Commun.* **2018**, *54*, 11041–11043.

(72) Ho, P. S. Biomolecular Halogen Bonds. In *Halogen Bonding I: Impact on Materials Chemistry and Life Sciences. Topics in Current Chemistry, Vol. 358*; Metrangolo, P., Resnati, G., Eds.; Springer International Publishing: Cham, 2014; pp 241–276.

(73) Ziegler, S.; Pries, V.; Hedberg, C.; Waldmann, H. Target identification for small bioactive molecules: finding the needle in the haystack. *Angew. Chem. Int. Ed.* **2013**, *52*, 2744–2792.

(74) Yang, Y.; Mahmoud, A. H.; Lill, M. A. Modeling of Halogen–Protein Interactions in Co-Solvent Molecular Dynamics Simulations. *J. Chem. Inf. Model.* **2019**, *59*, 38–42.

(75) Mahmoud, A. H.; Yang, Y.; Lill, M. A. Improving Atom-Type Diversity and Sampling in Cosolvent Simulations Using λ-Dynamics. *J. Chem. Theory Comput.* **2019**, *15*, 3272–3287.

(76) Nunes, R.; Vila-Viçosa, D.; Machuqueiro, M.; Costa, P. J. Biomolecular Simulations of Halogen Bonds with a GROMOS Force Field. *J. Chem. Theory Comput.* **2018**, *14*, 5383–5392.

(77) As no experimental value is available, the predicted average as reported in the CompTox Chemistry Dashboard (https://comptox.epa.gov/dashboard/) is presented.

(78) Williams, A. J.; Grulke, C. M.; Edwards, J.; McEachran, A. D.; Mansouri, K.; Baker, N. C.; Patlewicz, G.; Shah, I.; Wambaugh, J. F.; Judson, R. S., et al. The CompTox Chemistry Dashboard: a community data resource for environmental chemistry. *J. Cheminformatics* **2017**, *9*, 1–27.

(79) Ran, Y.; He, Y.; Yang, G.; Johnson, J. L.; Yalkowsky, S. H. Estimation of aqueous solubility of organic compounds by using the general solubility equation. *Chemosphere* **2002**, *48*, 487–509.

(80) Rowe, R. K.; Ho, P. S. Relationships between hydrogen bonds and halogen bonds in biological systems. *Acta Crystallogr. B* **2017**, *B73*, 255–264.

(81) Ibrahim, M. A. A. Molecular mechanical study of halogen bonding in drug discovery. *J. Comput. Chem.* **2011**, *32*, 2564–2574.

(82) Ibrahim, M. A. A. Performance Assessment of Semiempirical Molecular Orbital Methods in Describing Halogen Bonding: Quantum Mechanical and Quantum Mechanical/Molecular Mechanical-Molecular Dynamics Study. *J. Chem. Inf. Model.* **2011**, *51*, 2549–2559.

(83) Ibrahim, M. A. A. AMBER empirical potential describes the geometry and energy of noncovalent halogen interactions better than advanced semiempirical quantum mechanical method PM6-DH2X. *J. Phys. Chem. B* **2012**, *116*, 3659–3669.

(84) Ibrahim, M. A. A. Molecular mechanical perspective on halogen bonding. *J. Mol. Model.* **2012**, *18*, 4625–4638.

(85) Wang, J.; Wolf, R. M.; Caldwell, J. W.; Kollman, P. A.; Case, D. A. Development and testing of a general amber force field. *J. Comput. Chem.* **2004**, *25*, 1157–1174.

(86) Rosa, M.; Caltabiano, G.; Barreto-Valer, K.; Gonzalez-Nunez, V.; Gómez-Tamayo, J. C.; Ardá, A.; Jiménez-Barbero, J.; Pardo, L.; Rodríguez, R. E.; Arsequell, G.; Valencia, G. Modulation of the Interaction between a Peptide Ligand and a G Protein-Coupled Receptor by Halogen Atoms. *ACS Med. Chem. Lett.* **2015**, *6*, 872–876.

(87) Celis-Barros, C.; Saavedra-Rivas, L.; Salgado, J. C.; Cassels, B. K.; Zapata-Torres, G. Molecular dynamics simulation of halogen bonding mimics experimental data for cathepsin L inhibition. *J. Comput. Aided Mol. Des.* **2015**, *29*, 37–46.

(88) González-Vera, J. A.; Medina, R. A.; Martín-Fontecha, M.; Gonzalez, A.; de La Fuente, T.; Vázquez-Villa, H.; García-Cárceles, J.; Botta, J.; McCormick, P. J.; Benhamú, B.; Pardo, L.; López-Rodríguez, M. A new serotonin 5-HT6 receptor antagonist with procognitive activity–Importance of a halogen bond interaction to stabilize the binding. *Sci. Rep.* **2017**, *7*, 41293.

(89) Jiang, S.; Zhang, L.; Cui, D.; Yao, Z.; Gao, B.; Lin, J.; Wei, D. The Important Role of Halogen Bond in Substrate Selectivity of Enzymatic Catalysis. *Sci. Rep.* **2016**, *6*, 34750.

(90) Gautieri, A.; Milani, A.; Pizzi, A.; Rigoldi, F.; Redaelli, A.; Metrangolo, P. Molecular dynamics investigation of halogenated amyloidogenic peptides. *J. Mol. Model.* **2019**, *25*, 124.

(91) Lameira, J.; Bonatto, V.; Cianni, L.; dos Reis Rocho, F.; Leitão, A.; Montanari, C. A. Predicting the affinity of halogenated reversible covalent inhibitors through relative binding free energy. *Phys. Chem. Chem. Phys.* **2019**, *21*, 24723–24730.

(92) Bayly, C. I.; Cieplak, P.; Cornell, W. D.; Kollman, P. A. A well-behaved electrostatic potential based method using charge restraints for deriving atomic charges: the RESP model. *J. Chem. Phys.* **1993**, *97*, 10269–10280.

(93) Rendine, S.; Pieraccini, S.; Forni, A.; Sironi, M. Halogen bonding in ligand–receptor systems in the framework of classical force fields. *Phys. Chem. Chem. Phys.* **2011**, *13*, 19508–19516.

(94) Franchini, D.; Dapiaggi, F.; Pieraccini, S.; Forni, A.; Sironi, M. Halogen bonding in

the framework of classical force fields: The case of chlorine. *Chem. Phys. Lett.* **2018**, *712*, 89–94.

(95) Kolář, M.; Hobza, P. On extension of the current biomolecular empirical force field for the description of halogen bonds. *J. Chem. Theory Comput.* **2012**, *8*, 1325–1333.

(96) Kolář, M.; Hobza, P.; Bronowska, A. K. Plugging the explicit σ-holes in molecular docking. *Chem. Commun.* **2013**, *49*, 981–983.

(97) Titov, O. I.; Shulga, D. A.; Palyulin, V. A. Quadrupole Correction: From Molecular Electrostatic Potential to Free Energies of Halogen Bonding. *J. Chem. Theory Comput.* **2019**, *15*, 1159–1167.

(98) Jorgensen, W. L.; Schyman, P. Treatment of halogen bonding in the OPLS-AA force field: application to potent anti-HIV agents. *J. Chem. Theory Comput.* **2012**, *8*, 3895–3901.

(99) Harder, E. et al. OPLS3: a force field providing broad coverage of drug-like small molecules and proteins. *J. Chem. Theory Comput.* **2015**, *12*, 281–296.

(100) Roos, K.; Wu, C.; Damm, W.; Reboul, M.; Stevenson, J. M.; Lu, C.; Dahlgren, M. K.; Mondal, S.; Chen, W.; Wang, L.; Abel, R.; Friesner, R. A.; Harder, E. D. OPLS3e: Extending force field coverage for drug-like small molecules. *J. Chem. Theory Comput.* **2019**, *15*, 1863–1874.

(101) Gutiérrez, I. S.; Lin, F.-Y.; Vanommeslaeghe, K.; Lemkul, J. A.; Armacost, K. A.; Brooks, C. L.; MacKerell, A. D. Parametrization of halogen bonds in the CHARMM general force field: Improved treatment of ligand–protein interactions. *Bioorg. Med. Chem.* **2016**, *24*, 4812–4825.

(102) Zhou, Y.; Wang, Y.; Li, P.; Huang, X.-P.; Qi, X.; Du, Y.; Huang, N. Exploring Halogen

Bonds in 5-Hydroxytryptamine 2B Receptor–Ligand Interactions. *ACS Med. Chem. Lett.* **2018**, *9*, 1019–1024.

(103) Nunes, R.; Vila-Viçosa, D.; Costa, P. J. Tackling Halogenated Species with PBSA: Effect of Emulating the σ–Hole. *J. Chem. Theory Comput.* **2019**, *15*, 4241–4251.

(104) Luchi, A. M.; Angelina, E. L.; Andujar, S. A.; Enriz, R. D.; Peruchena, N. M. Halogen bonding in biological context: a computational study of D2 dopamine receptor. *J. Phys. Org. Chem.* **2016**, *29*, 645–655.

(105) Rana, N.; Conley, J. M.; Soto-Velasquez, M.; Leon, F.; Cutler, S. J.; Watts, V. J.; Lill, M. A. Molecular Modeling Evaluation of the Enantiomers of a Novel Adenylyl Cyclase 2 Inhibitor. *J. Chem. Inf. Model.* **2017**, *57*, 322–334.

(106) Costa, P. J.; Nunes, R. Advances in the Computational Modeling of Halogen Bonds in Biochemical Systems. In *Frontiers in Computational Chemistry: Volume 4*; Ul-Haq, Z., Wilson, A. K., Eds.; Bentham Science Publishers: Sharjah, UAE, 2018; Chapter 4, pp 144–183.

(107) Carter, M.; Rappé, A. K.; Ho, P. S. Scalable anisotropic shape and electrostatic models for biological bromine halogen bonds. *J. Chem. Theory Comput.* **2012**, *8*, 2461–2473.

(108) Scholfield, M. R.; Ford, M. C.; Vander Zanden, C. M.; Billman, M. M.; Ho, P. S.; Rappé, A. K. Force field model of periodic trends in biomolecular halogen bonds. *J. Phys. Chem. B* **2015**, *119*, 9140–9149.

(109) Santos, L. A.; da Cunha, E. F.; Ramalho, T. C. Toward the classical description of halogen bonds: a quantum based generalized empirical potential for fluorine, chlorine, and bromine. *J. Phys. Chem. A* **2017**, *121*, 2442–2451.

(110) Du, L.; Gao, J.; Bi, F.; Wang, L.; Liu, C. A polarizable ellipsoidal force field for halogen bonds. *J. Comput. Chem.* **2013**, *34*, 2032–2040.

(111) Mu, X.; Wang, Q.; Wang, L.-P.; Fried, S. D.; Piquemal, J.-P.; Dalby, K. N.; Ren, P. Modeling organochlorine compounds and the σ-hole effect using a polarizable multipole force field. *J. Phys. Chem. B* **2014**, *118*, 6456–6465.

(112) Lin, F.-Y.; MacKerell Jr, A. D. Improved Modeling of Halogenated Ligand–Protein Interactions Using the Drude Polarizable and CHARMM Additive Empirical Force Fields. *J. Chem. Inf. Model.* **2018**, *59*, 215–228.

(113) Hariharan, P. C.; Pople, J. A. The influence of polarization functions on molecular orbital hydrogenation energies. *Theor. Chim. Acta* **1973**, *28*, 213–222.

(114) Francl, M. M.; Pietro, W. J.; Hehre, W. J.; Binkley, J. S.; Gordon, M. S.; DeFrees, D. J.; Pople, J. A. Self-consistent molecular orbital methods. XXIII. A polarization-type basis set for second-row elements. *J. Chem. Phys.* **1982**, *77*, 3654–3665.

(115) Rassolov, V. A.; Ratner, M. A.; Pople, J. A.; Redfern, P. C.; Curtiss, L. A. 6-31G* basis set for third-row atoms. *J. Comput. Chem.* **2001**, *22*, 976–984.

(116) Glukhovtsev, M. N.; Pross, A.; McGrath, M. P.; Radom, L. Extension of Gaussian-2 (G2) theory to bromine-and iodine-containing molecules: Use of effective core potentials. *J. Chem. Phys.* **1995**, *103*, 1878–1885.

(117) Frisch, M. J. et al. Gaussian 09 Revision D.01. Gaussian Inc. Wallingford CT 2009.

(118) The MK atomic radius for iodine is unknown in Gaussian09. Therefore, the default atomic radius for bromine (2.3 Å) was assigned.

(119) Wang, J.; Wang, W.; Kollman, P. A.; Case, D. A. Automatic atom type and bond type perception in molecular mechanical calculations. *J. Mol. Graph. Model.* **2006**, *25*, 247–260.

(120) Case, D. A. et al. AMBER 2015. University of California, San Francisco, 2015.

(121) da Silva, A. W. S.; Vranken, W. F. ACPYPE-AnteChamber PYthon Parser interfacE. *BMC Res. Notes* **2012**, *5*, 367.

(122) Berendsen, H. J. C.; van der Spoel, D.; van Drunen, R. GROMACS: a message-passing parallel molecular dynamics implementation. *Comput. Phys. Commun.* **1995**, *91*, 43–56.

(123) Van Der Spoel, D.; Lindahl, E.; Hess, B.; Groenhof, G.; Mark, A. E.; Berendsen, H. J. C. GROMACS: fast, flexible, and free. *J. Comput. Chem.* **2005**, *26*, 1701–1718.

(124) Abraham, M. J.; Murtola, T.; Schulz, R.; Páll, S.; Smith, J. C.; Hess, B.; Lindahl, E. GROMACS: high performance molecular simulations through multi-level parallelism from laptops to supercomputers. *SoftwareX* **2015**, *1*, 19–25.

(125) Dickson, C. J.; Madej, B. D.; Skjevik, Å. A.; Betz, R. M.; Teigen, K.; Gould, I. R.; Walker, R. C. Lipid14: The Amber Lipid Force Field. *J. Chem. Theory Comput.* **2014**, *10*, 865–879.

(126) Jorgensen, W. L.; Chandrasekhar, J.; Madura, J. D.; Impey, R. W.; Klein, M. L. Comparison of simple potential functions for simulating liquid water. *J. Chem. Phys.* **1983**, *79*, 926–935.

(127) Bussi, G.; Donadio, D.; Parrinello, M. Canonical sampling through velocity rescaling. *J. Chem. Phys.* **2007**, *126*, 014101.

(128) Berendsen, H. J.; Postma, J. v.; van Gunsteren, W. F.; DiNola, A.; Haak, J. R. Molecular dynamics with coupling to an external bath. *J. Chem. Phys.* **1984**, *81*, 3684–3690.

(129) Darden, T.; York, D.; Pedersen, L. Particle mesh Ewald: an $N{\cdot}\log(N)$ method for Ewald sums in large systems. *J. Chem. Phys.* **1993**, *98*, 10089–10092.

(130) Essmann, U.; Perera, L.; Berkowitz, M. L.; Darden, T.; Lee, H.; Pedersen, L. G. A smooth particle mesh Ewald method. *J. Chem. Phys.* **1995**, *103*, 8577–8593.

(131) Pall, S.; Hess, B. A flexible algorithm for calculating pair interactions on SIMD architectures. *Comput. Phys. Commun.* **2013**, *184*, 2641–2650.

(132) Hess, B. P-LINCS: A Parallel Linear Constraint Solver for Molecular Simulation. *J. Chem. Theory Comput.* **2008**, *4*, 116–122.

(133) Hess, B.; Bekker, H.; Berendsen, H. J.; Fraaije, J. G. LINCS: a linear constraint solver for molecular simulations. *J. Comput. Chem.* **1997**, *18*, 1463–1472.

(134) Miyamoto, S.; Kollman, P. A. SETTLE: an analytical version of the SHAKE and RATTLE algorithm for rigid water models. *J. Comput. Chem.* **1992**, *13*, 952–962.

(135) Kučerka, N.; Nieh, M.-P.; Katsaras, J. Fluid phase lipid areas and bilayer thicknesses of commonly used phosphatidylcholines as a function of temperature. *BBA Biomembranes* **2011**, *1808*, 2761–2771.

(136) Silverman, B. W. *Density estimation for statistics and data analysis*; Monographs on Statistics and Applied Probability; Chapman and Hall: London, 1986.

(137) Campos, S. R. R.; Baptista, A. M. Conformational analysis in a multidimensional energy landscape: study of an arginylglutamate repeat. *J. Phys. Chem. B* **2009**, *113*, 15989–16001.

(138) The PyMOL Molecular Graphics System, Version 2.0 Schrödinger, LLC.

(139) Zhang, Q.; Xu, Z.; Zhu, W. The underestimated halogen bonds forming with protein side chains in drug discovery and design. *J. Chem. Inf. Model.* **2017**, *57*, 22–26.

(140) Lu, Y.; Wang, Y.; Zhu, W. Nonbonding interactions of organic halogens in biological systems: implications for drug discovery and biomolecular design. *Phys. Chem. Chem. Phys.* **2010**, *12*, 4543–4551.

Graphical TOC Entry